Dalton Transactions

Accepted Manuscript

This article can be cited before page numbers have been issued, to do this please use: W. J. Roth, B. Gil, A. Mayoral, J. Grzybek, A. Korzeniowska, M. Kubu, W. Makowski, J. Cejka, Z. Olejniczak and M. Mazur, *Dalton Trans.*, 2017, DOI: 10.1039/C7DT03718J.

This is an Accepted Manuscript, which has been through the Royal Society of Chemistry peer review process and has been accepted for publication.

Accepted Manuscripts are published online shortly after acceptance, before technical editing, formatting and proof reading. Using this free service, authors can make their results available to the community, in citable form, before we publish the edited article. We will replace this Accepted Manuscript with the edited and formatted Advance Article as soon as it is available.

You can find more information about Accepted Manuscripts in the author guidelines.

Please note that technical editing may introduce minor changes to the text and/or graphics, which may alter content. The journal's standard Terms & Conditions and the ethical guidelines, outlined in our author and reviewer resource centre, still apply. In no event shall the Royal Society of Chemistry be held responsible for any errors or omissions in this Accepted Manuscript or any consequences arising from the use of any information it contains.

ROYAL SOCIETY OF CHEMISTRY

rsc.li/dalton

View Article Online
DOI: 10.1039/C7DT03718J

Pillaring of layered zeolite precursors with ferrierite topology leading to unusual molecular sieves on the micro/mesoporous border

Wieslaw J. Roth,[1] Barbara Gil,[1] Alvaro Mayoral,[2] Justyna Grzybek,[1] Aleksandra Korzeniowska,[1] Martin Kubu,[3] Wacław Makowski,[1] Jiří Čejka[3] , Zbigniew Olejniczak[4], Michal Mazur[5,6]

[1]*Faculty of Chemistry, Jagiellonian University in Kraków, Gronostajowa 2, 30-387 Kraków, Poland*
[2] *Laboratorio de Microscopias Avanzadas (LMA), Instituto de Nanociencia de Aragón (INA), Universidad de Zaragoza, 50018 Zaragoza, Spain*
[3]*J. Heyrovský Institute of Physical Chemistry, Academy of Sciences of the Czech Republic, Dolejškova 3, CZ-182 23 Prague, Czech Republic*
[4]*Institute of Nuclear Physics, Radzikowskiego 152, 31-342 Kraków, Poland*
[5]*Department of Physical and Macromolecular Chemistry, Faculty of Science, Charles University, Hlavova 2030/8, CZ-128 43 Prague, Czech Republic*
[6] *EaStCHEM School of Chemistry, University of St Andrews, St Andrews KY16 9ST, UK*

Abstract

Layered zeolite materials with FER layer topology can produce various condensed and expanded structures including zeolite frameworks FER and CDO, their interlayer expanded forms (IEZ), and organic-intercalated and pillared derivatives. This work concerns pillaring of the surfactant-swollen derivative with ca. 2.5 nm gallery height between layers by treatment with tetraethylorthosilicate (TEOS) at room and elevated temperatures. The materials obtained at 100 °C and higher showed unusual properties including 2 nm pores on the micro/mesoporous border and disordered layer packing indicated by the absence of distinct low angle interlayer peaks at d-spacing >3 nm (~3° 2-θ Cu Kα radiation) in the X-ray diffraction pattern (XRD). TEOS treatment at room temperature produced a pillared molecular sieve with the expected mesoporous characteristics, namely pore size around 3 nm and high intensity low angle (001) peak at 2.3° 2-θ, 3.8 nm d-spacing, in the XRD. The characterization aiming to elucidate the nature of the obtained unusual products included gas adsorption isotherms, aberration corrected (Cs-corrected) Scanning Transmission Electron Microscopy (STEM) studies and ^{29}Si solid state NMR. BET surface area values decreased with the temperature of TEOS treatment from approximately 1200 m^2/g to ~900 and 600 m^2/g, for the room temperature, 100 °C, and 120 °C, respectively. The ^{29}Si solid state NMR revealed presence of both Q^3 ($(SiO)_3SiOX$, X=H or minus charge) and Q^4 ($(SiO)_4Si$) centers giving separated signals up to the pillaring step. After pillaring at 100 °C and calcination the nominal intensity ratios Q^4:Q^3 were 2.17 and 2.61 but the signals were merged into one broad peak indicating structural heterogeneity of Si-O coordination. The microscopy showed the presence of FER layers in the samples but the overall structure and composition were not well-defined. The observed unusual disorganization and possible partial degradation of layers during pillaring may result from the combination of high temperature, alkalinity (surfactant hydroxide) and siliceous composition of the layers. The obtained pillared products are of interest for preparation of larger pore catalysts and sorbents or controlled drug delivery.

View Article Online
DOI: 10.1039/C7DT03718J

Introduction

The ability of various solids to intercalate[1-3] or, more generally, reversibly absorb external molecules has been exploited in many technological processes such as sorption,[4] separation,[5] heterogeneous catalysis[6-8] and others.[9] These solids are called hosts while the sorbates or reagents are guest molecules. Hosts are classified according to structural dimensionality of their components from 0 to 3 as follows: discrete molecules as 0D, chains – 1D, layers – 2D and frameworks – 3D.[2,10] The lower-dimensional solids are profoundly different from the 3D ones – they have flexible structures composed of rigid building blocks and in principle can be spatially modified, for example by intercalation. 3D frameworks are embodied by zeolites, which have rigid structures containing discrete micropores.[11] They exhibit exceptional selective sorption properties and catalytic activity, especially as solid acids,[12] and many technologies are based on their use.[13,14] The available useful zeolites exhibit pores no greater than about 1 nm. This prompted development of procedures for synthesis of larger pore molecular sieve materials by expansion and fixing in 3D of suitable 2D layered materials.[15,16] This approach is often referred to as swelling and pillaring.

As a major breakthrough, amounting to a paradigm shift or at least its expansion, was the finding that zeolite frameworks can be synthesized as 2D solids consisting of 1-3 nm layers in assemblies from ordered to disordered.[17-21] There are now about 20 frameworks out of 235 approved by the International Zeolite Association (IZA) Structure Commission demonstrating some layered form.[22,23] The principal forms of 2D zeolites are layered precursors, which can undergo topotactic condensation producing complete, ordered 3D zeolite frameworks.[24,25] This provides the second synthesis pathway to 3D frameworks in addition to the conventional direct one by which most zeolites have been obtained.[26] Thirteen out of the 235 IZA approved zeolite frameworks have been found so far to form such precursors and 5 of them have been obtained only by the indirect precursor route.[27] The initial zeolite layered forms were obtained usually by accident but there are now examples of preparation by design, e.g. multi-lamellar and unilamellar MFI zeolite nanosheets[28,29] and by top-down approach designated ADOR[30-32] meaning Assembly-Disassembly-Organization-Reassembly, i.e. synthesis of a suitable 3D zeolite (assembly), disassembly into 2D lamellae,[33] organization/alignment of the layers and reassembly into a new framework .

The 2D zeolite discovery and progress offered significant practical benefits by providing layers with high catalytic activity and pores in and across layers.[34,35] These were characteristics generally lacking in the conventional 2D solids. The application of post-synthesis modification procedures such as swelling (expansion by intercalation), pillaring, delamination and others, that were previously developed with layered solids in general,[36] have been extended to some 2D zeolites. They produced new materials with high zeolite-like catalytic activity[8,34] and enabled 3D mass transport of molecules.[35] In addition to these anticipated effects, layered zeolites revealed unpredicted phenomena exemplified by formation of more than one zeolite framework from the same layer when its structure allows it[37] and the preparation of so-called interlayer expanded zeolites denoted IEZ by silylation.[38,39] The latter are unprecedented ordered pillared structures mainly with two-atom (metal and oxygen) bridge.

View Article Online
DOI: 10.1039/C7DT03718J

The above two new effects are demonstrated by the layers having topology of zeolite FER,[20] which are the subject of this article. In addition to the framework FER these layers also give in a different configuration zeolite CDO,[40,41] as well as materials with incomplete structures like ERS-12.[42] The framework structure FER is a well-known, classical zeolite ferrierite, that was found in nature first[43] and is useful in catalysis.[44] The initial accidental synthesis of the layered FER precursor[20] validated the concept of 2D zeolites, first identified with MCM-22,[45] as a more general phenomenon, possibly applicable to all frameworks.[26]

In the present work, we report results related to swelling and pillaring of the FER layers. These treatments are routinely carried out to produce expanded layered structures[16,19] but the behavior observed in this case was unusual and more complex justifying special attention. Specifically, pillaring revealed unexpected strong dependence on the temperature of treatment with the pillaring agent, TEOS and afforded unusual pillared materials with narrow pore size distribution on the border between micro- and mesopores. The obtained products were characterized to establish their properties and to learn more about factors affecting the pillaring process, especially the unexpected behavior.

Results and discussion

1. Synthesis and properties of the FER layers

Various layered precursors containing FER layers were synthesized by conventional hydrothermal methods with different organic structure directing agents (SDA).[24,46,47] The products have platelet morphology with ordered or semi-ordered stacks of about 1 nm thick FER layers with SDA molecules in the interlayer region. A detailed report by Marler[46] shows that relative lateral positioning of the layers is strongly influenced by the SDA molecules, which in turn determines the structure of the final condensed material produced upon calcination. The obtained materials included ordered 3D frameworks FER and CDO, partially ordered incomplete structures like ERS-12[42] and solids with apparently non-periodic intractable structure. The latter may include apparently collapsed stacks, so-called sub-FER, with interlayer d-spacing repeat shorter than in the complete 3D framework.[48]

View Article Online
DOI: 10.1039/C7DT03718J

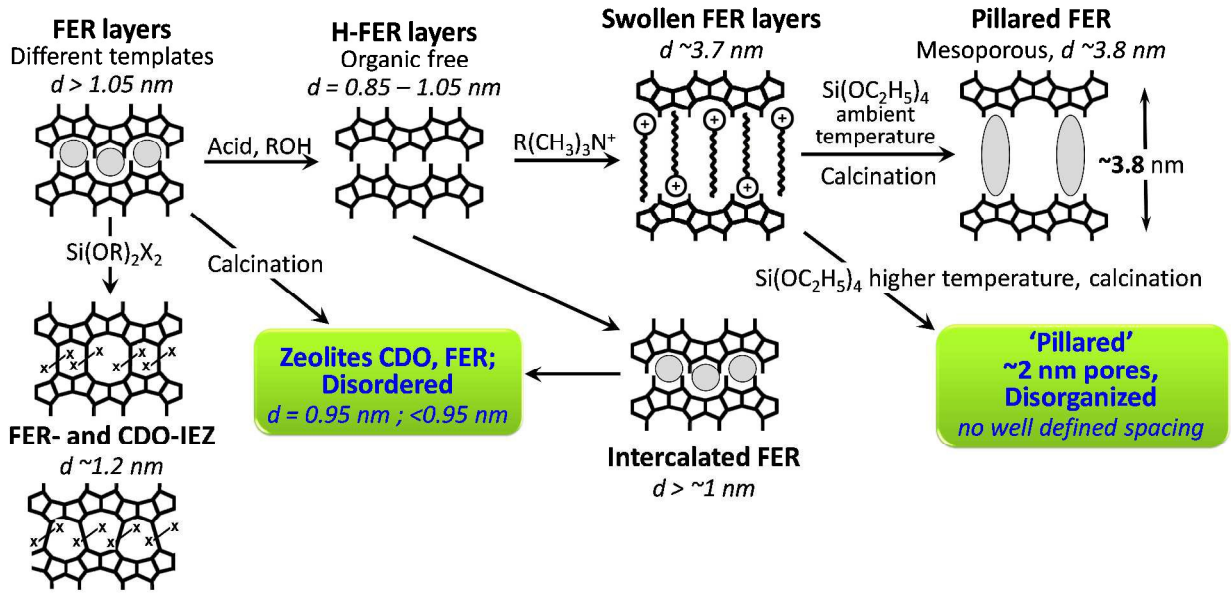

Figure 1. Schematic representation of the basic transformations of the layered materials with FER structure. The pillared products on the right are the subject of this work. The provided 'd' values are approximate interlayer d-spacings observed for the corresponding materials.

The material used in this work is a borosilicate obtained with choline as the structure directing agent.[49] The as-synthesized product is designated ZSM-55 and it condenses to the CDO topology upon calcination.[41] The layers with FER structure can interconvert between FER and CDO arrangements but can also produce non-congruent (unsymmetric, without exact matching of all silanols on opposing layers) or disordered stacking, especially after treatments.[47,50] This may invalidate the original designations as FER or CDO precursors. We will adopt the term 'FER layers' as generic description for all materials.

The as-synthesized precursor ZSM-55 can be contacted with a mineral acid such as hydrochloric or nitric in alcohol to remove the SDA leading to an organic-free precursor,[51] referred to as H-ZSM-55.[47] This enables subsequent intercalation of other organic compounds in particular to obtain a swollen product with greatly expanded interlayer distance, e.g. by 2.5 nm with hexadecyltrimethylammonium (HDTMA) cation.[50,52] Residual boron present in ZSM-55 is also extracted in the acid medium making H-ZSM-55 an all-silica product.

2. Identification of products by X-ray powder diffraction

Figure 2 shows X-ray diffraction patterns of the studied materials, presented separately for the low angle range (below 10° 2-θ, CuKα radiation throughout) and for higher angles. The precursor ZSM-55 produces CDO zeolite upon calcination. [17,47] ZSM-55 transformation to the organic-free layered product was confirmed by XRD on the basis of overall peak broadening and shifting of the peak (00l) near 8.3° 2-θ to higher angles upon drying above room temperature. Successful swelling with the surfactant hydroxide solution at high pH (~12.5) was confirmed by the new dominant low angle line at 2.7° 2-θ (3.5 nm) and the absence of the initial low angle line reflection at 8.3° 2-θ (1.1 nm).

View Article Online
DOI: 10.1039/C7DT03718J

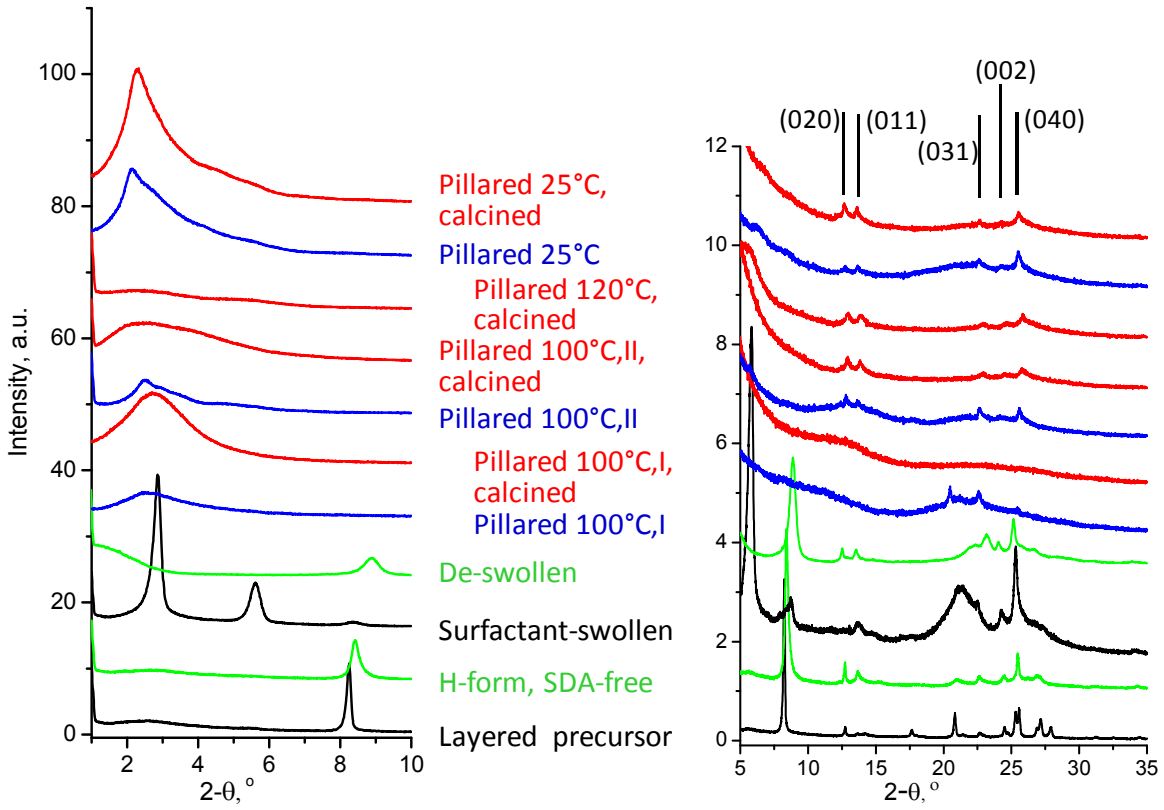

Figure 2. XRD pattern of the materials reported in this work. The principal intralayer reflections of the FER layer are identified based on the reference.[20] Assignment of the other reflections is uncertain or impossible, except for the lowest angle peaks corresponding to interlayer separations.

To verify that swelling did not destroy the FER layers and no surfactant-templated mesophases were formed, the swollen sample was contacted with a solution of ammonium nitrate in alcohol, which extracted the intercalated surfactant. XRD of the 'deswollen' sample showed recovered low angle peak near 8.3° 2-θ and other reflections identifying the FER layers. This proves overall preservation of the integrity of the layers but ^{31}Si MAS NMR, discussed later, indicates formation of additional Q^3 (silanol) defects.

3. Pillaring with TEOS

Treatment with TEOS was developed in the 1990s as a particularly reliable method of pillaring and for obtaining permanent separation of layers in expanded (swollen) layered materials. [16] If no pillaring treatment is applied, the removal of the swelling agent by extraction or calcination results in collapse to the original unexpanded state. During pillaring with TEOS, silicon oxide precursors are intercalated and partially hydrolyzed in the interlayer space, producing permanent oxide props at higher temperatures. The obtained products often exhibit relatively narrow pore size distribution in the mesoporous range. Pillaring treatments are usually carried out at elevated temperature, typically above 50 °C, with the

View Article Online
DOI: 10.1039/C7DT03718J

option of subsequent contacting with water (hydrolysis) or not, prior to calcination.[52] This treatment is considered to have been successful when the original low angle reflection (after swelling), which is indicative of large gallery height, is maintained. Usually this peak is broadened in comparison to the swollen product but its presence proves preservation of the initial, largely parallel and roughly equidistant layer stacking. The XRD evaluation is used in conjunction with the measurement of BET surface area or other quantitative texture determinations, which should show meaningful enhancement as evidence of successful pillaring.

Pillaring of the swollen precursors with FER layers showed enormous difference depending on the temperature of treatment. The reaction at room temperature yielded the product with preserved low angle line around 2.3° 2-θ (3.8 nm d-spacing) and the original layer stacking. The samples contacted with TEOS at elevated temperatures (here 100 °C or higher) showed, in most instances, greatly diminished quality of the XRD pattern, especially with regard to the prominent (001) low angle peak seen in swollen materials at 2.8° 2-θ (3.2 nm d-spacing). Reflections in that region had reduced intensity and were broadened up to being hardly distinguishable. This we interpret as a loss or significant reduction of the periodic stacking order in the mesoscale. This was surprising because texture determination indicated narrow pore size distribution characteristics. XRD patterns at higher angles contained maxima corresponding to FER layers confirming preservation of their internal structure. The corresponding reflections are identified as follows: (020) at 12.6°, (011) at 13.5°, (031) at 22.5°, (040) at 25.4° 2-θ (positions in degrees are approximate and can vary).[20]

4. Gas adsorption and pore size determinations

Adsorption isotherms of the materials obtained from the layered precursor are shown in Figure 3, while corresponding textural parameters are listed in Table 1. The adsorption capacity of 3D zeolite CDO produced upon calcination of ZSM-55 is quite a small but it is significantly enhanced in the stabilized IEZ form. All TEOS treated derivatives have much higher adsorption capacity confirming successful pillaring. The highest adsorption capacity was obtained by TEOS treatment at room temperature and the isotherm profile is typical for mesoporous pillared solids.

The isotherms for products pillared at higher temperatures are different not only based on quantitative but also qualitative characteristics. Their profiles have the following notable features: (i) steep uptake in the 'microporous' range up to $p/p_0<0.1$, (ii) quickly leading to a plateau and (iii) no adsorption/ desorption hysteresis.

Table 1. Porosity parameters obtained from nitrogen isotherm plots and nonane Quasi Equilibrated Temperature-Programmed Desorption and Adsorption (QE-TPDA) measurements.*

Material	S_{BET}[1] (m^2/g)	S_{EXT}[2] (m^2/g)	$V_{T\text{-}PLOT}$[2] (m^2/g)	V_{TOT}[3] (cm^3/g)	D_{DFT}[4] (nm)	$V_{QE\text{-}TPDA}$[5] (cm^3/g)	$D_{QE\text{-}TPDA}$[5] (nm)
CDO, ZSM-55	71	17	0.02	0.05	-	0.02	-
CDO-IEZ	374	43	0.15	0.20	-	0.11	-
Pillared, 20°C	1194	72	0.56	0.69	2.9	0.37	2.1
Pillared, 100°C,I	955	66	0.40	0.52	na	0.30	1.3

View Article Online
DOI: 10.1039/C7DT03718J

Pillared, 100°C, II	857	59	0.37	0.47	1.9	na	na
Pillared, 120°C	604	51	0.26	0.33	1.7	0.21	0.8

*Based on N_2 sorption: [1]total BET method, [2]external surface area and pore volume by *t*-plot method (combining micropores and small mesopores), [3] total volume at $p/p_0 = 0.95$, [4] Pore size maximum by DFT method; [5] Pore volume and pore size based on QE-TPDA of nonane. na – not available. CDO and CDO-IEZ contain negligible mesopores.

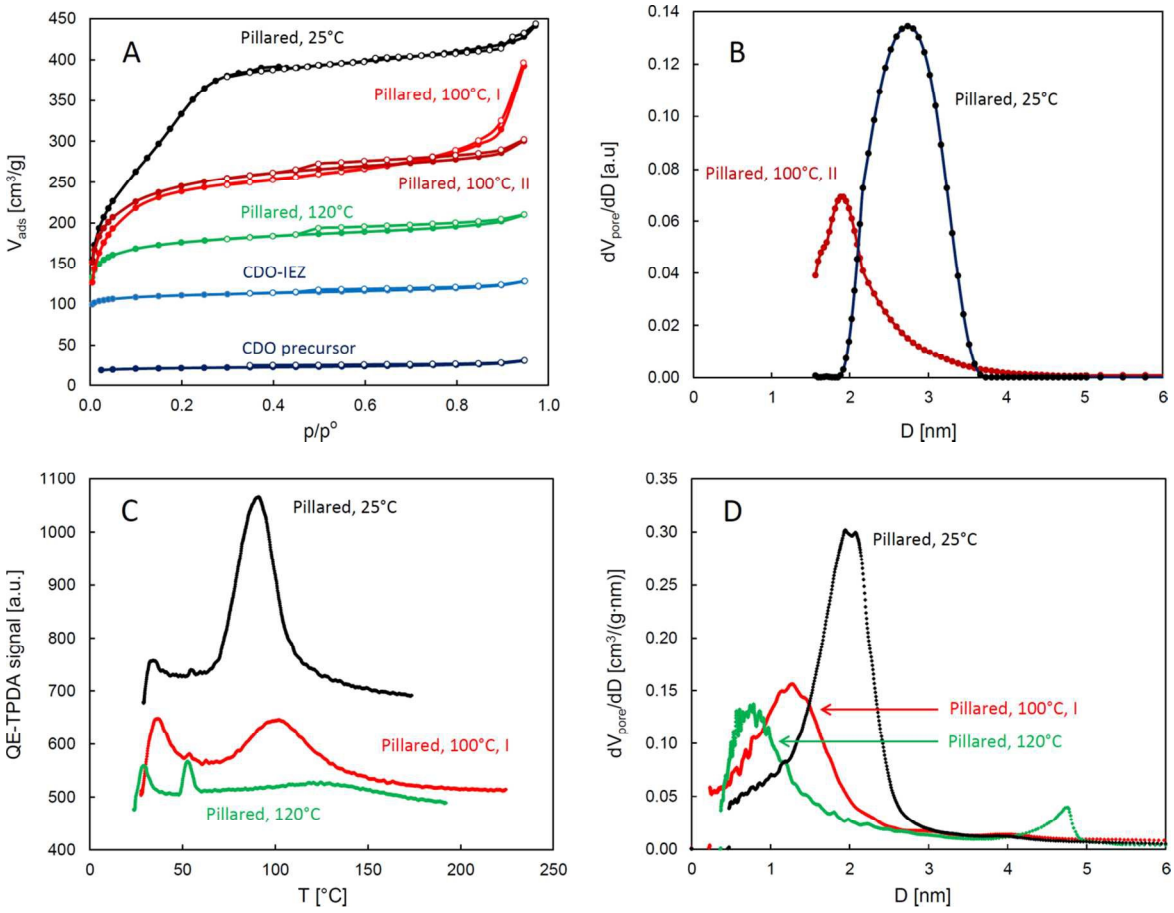

Figure 3. Representative nitrogen adsorption/desorption isotherms (A) and pore size distributions determined by Ar physisorption (B), desorption parts of the QE-TPDA profiles of nonane (C) and the corresponding pore size distributions (D).

Pore size calculations using standard Micromeritics DFT algorithms (see Experimental Section) showed narrow pore size distributions, with somewhat variable position of the maximum but generally around 2 nm. This value is a micro- mesopore divide established by IUPAC, and pore size of 2 nm is not readily achieved by design. The products are also useful as different pore sized materials derived from the same zeolite layer. Such series of similar materials with different pores can be considered for controlled drug delivery studies.

Pore size characteristics were also determined by Quasi Equilibrated Temperature-Programmed Desorption and Adsorption (QE-TPDA)[53] with nonane as the probe molecule.[54] The obtained profiles (Figure 3C), exhibiting strong desorption maxima at 80-120 °C corresponding to small mesopores or

View Article Online
DOI: 10.1039/C7DT03718J

large micropores, were consistent with the static nitrogen sorption results. The lack of high temperature maxima (above 150 °C) in the QE-TPDA profiles indicates that the studied samples do not contain micropores typical for zeolites. [55] The values of pore sizes calculated from the QE-TPDA profiles (Table 1) are underestimated due to the fact that such small pores are beyond applicability range of the BJH scheme used. However, these values and the pore size distributions (Figure 3D) follow the trend determined by DFT analysis of Ar sorption isotherms and represent well differences in porosity of the studied materials.

5. Aberration corrected (C_s-corrected) Scanning Transmission Electron Microscopy (STEM) studies

For the pillared material treated with TEOS at room temperature it is reasonable to assign the model of parallel layers represented in Figure 1 by the upper right structure. The pillared samples obtained by the reaction with TEOS at elevated temperature have unknown structure and were investigated by C_s-corrected STEM using a high annular dark field detector (HAADF); in both precalcined and calcined forms. The representative images are shown in Figure 4. We are unable to propose a model for the structure based on the images obtained. Features attributable to FER layers edge-on were observed, including domains with multiple parallel stacking, indicating that some parts preserved the original structure produced by swelling. But there were also domains with unseparated layers and portions that could not be interpreted. The observed features do not show a direct connection between pore size distributions and structural observations in the C_s-corrected STEM microscope.

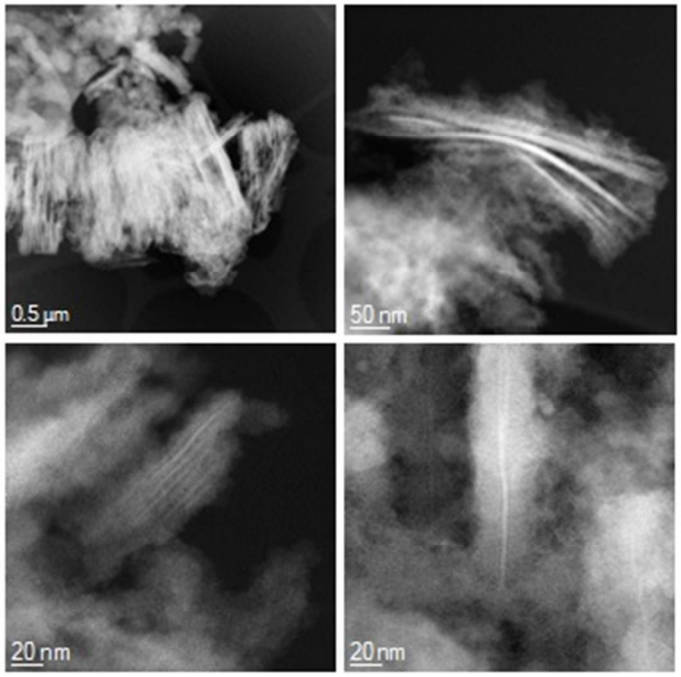

Figure 4a. C_s-corrected STEM-HAADF images of the uncalcined pillared 100 (swollen, TEOS treated at 100 °C) layered FER materials.

View Article Online
DOI: 10.1039/C7DT03718J

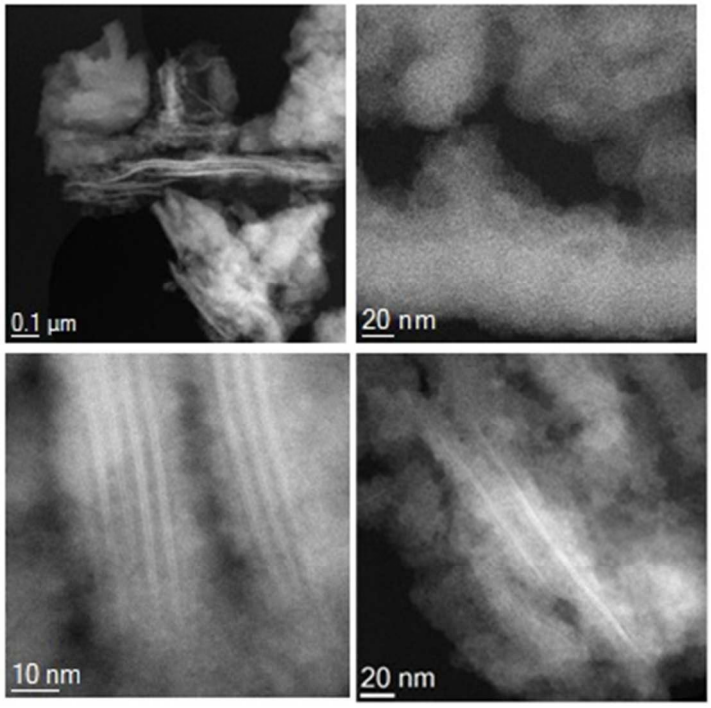

Figure 4b. C_s-corrected STEM-HAADF images of the calcined pillared at 100 °C layered FER materials shown at different magnifications.

6. Solid state ^{29}Si NMR

The spectra obtained for selected samples are shown in Figure 5. The idealized FER layer contains four Q^3 Si atoms as $(SiO)_3Si$-X, where X = OH, or O^-, and 14 Q^4 Si atoms as $(SiO)_4Si$, giving the ratio 1:3.5 for the corresponding ^{29}Si NMR signals.[46] Their expected positions are near -102 and -112 ppm, respectively, but are often composed of more than one component. The ratio Q^4:Q^3 for as-synthesized ZSM-55 is equal to 3.07 to 1 and it approaches the idealized ratio. The deviation from 3.5 is probably due to additional Q^3 defects, which are likely to form during synthesis. Calcination induces predominantly congruent condensation of silanols but leaves residual silanols/defects indicated by the ratio 22:1 (about 4.5 % of total). The percentage of silanols (Q^3 silicas) increases as a result of template extraction with acid and reaches nearly 40 % upon swelling treatment with HDTMA-OH (Q^3:Q^4 ratio changed to 1:1.43) indicating that swelling generates additional SiO^-/SiOH groups out of the Q^4 silicon atoms. We examined 2 samples pillared at 100 °C and found that the ratios Q^4 to Q^3 increased to above 2. A notable feature is the lack of resolution of the Q^3 and Q^4 signals and general broadening indicative of heterogeneity of Si-O-Si angles. TEOS is the likely source of these effects.

View Article Online
DOI: 10.1039/C7DT03718J

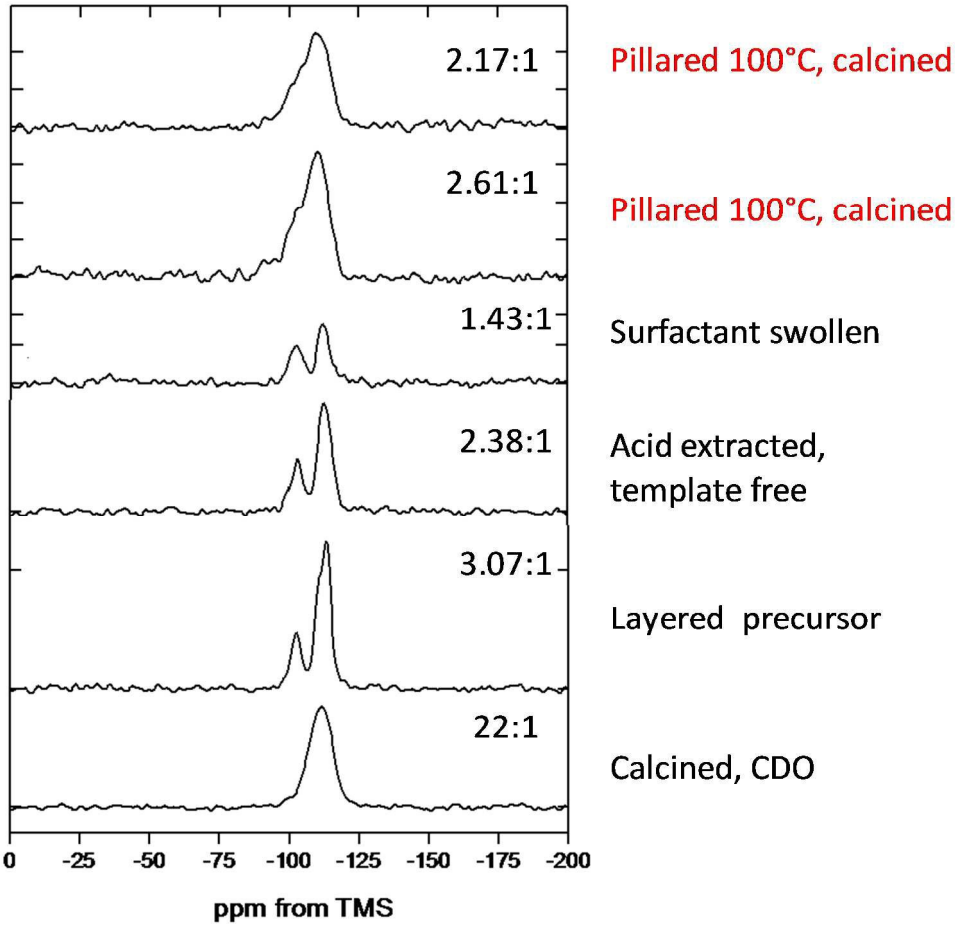

Figure 5. Solid state ^{29}Si MAS NMR of selected materials with calculated Q^4 Si to Q^3 Si ratios, based on peak deconvolution, shown on the right. The chemical shift value separating these two environments is equal to -105 ppm.

In summary, solid state ^{29}Si NMR provides valuable insight into properties and behavior of the layered FER systems but has not given additional clues about nature of the unusual pillared products obtained at higher temperature.

Conclusions

Pillaring of surfactant-swollen layered zeolite material with FER topology by treatment with tetraethyl orthosilicate (TEOS) gave different types of materials depending on temperature. TEOS treatment at room temperature produced a pillared molecular sieve with the expected structure consisting of stacked layers with about 2.5 nm gallery heights and approximately 3 nm mesopores. X-ray diffraction pattern of this material contained high intensity low angle (001) peak at 2.3° 2-θ, 3.8 nm d-spacing. The products obtained at temperatures 100 °C and higher showed disordered layer packing indicated by the absence of well defined XRD peaks above 3 nm d-spacing. The materials pillared at 100 °C had 2 nm pores on the micro/mesoporous border. They were examined by aberration corrected (Cs-corrected) Scanning Transmission Electron Microscopy (STEM), which confirmed the presence of FER layers but without any

View Article Online
DOI: 10.1039/C7DT03718J

pattern that might reveal internal structure and explain the observed pore characteristics. These results indicated that pillaring at higher temperature causes disorganization and possibly partial layer degradation. Similar effects at room temperature are much less severe and well defined pillared structure is obtained. The ^{29}Si solid state NMR showed the presence of both Q^3 ($(SiO)_3SiOX$, X=H or minus charge) and Q^4 ($(SiO)_4Si$) centers giving separated signals initially. The ratio Q^4 : Q^3 was equal to ~3:1 in the as-synthesized layered precursor and decreased to 1.43:1 after swelling. After pillaring at 100 °C and calcination the nominal intensity ratios Q^4:Q^3 were in two samples 2.17 and 2.61 but the signals were merged into one broad peak indicating structural heterogeneity of the Si-O coordination. BET surface area values decreased with the temperature of TEOS treatment from approximately 1200 m^2/g to ~900 and 600 m^2/g, for the room temperature, 100 °C, and 120 °C, respectively. The obtained pillared products are of interest for preparation of larger pore catalysts, e.g. as supports or by functionalization, and sorbents or controlled drug delivery. In the latter, different pore sizes may allow selection of most favorable interaction with guest molecules.

Experimental

Synthesis

ZSM-55 was prepared and transformed into the template-free and swollen derivatives as described earlier.[17,47] The following exemplifies typical preparations. ZSM-55 synthesis mixture: 1.36 g boric acid in 120 g of water, 10 g of 50 % NaOH, 40 g choline chloride and 65 g Ludox LS30; heated at 150°C with rotation for 90 hrs. Template extraction involved contacting 3-5 g of ZSM-55 with 100 ml of 3 M HCl in methanol at 50 °C for overnight. The obtained product was swollen at room temperature with a 50/50 mixture of solutions of 25 % hexadecyltrimethylammonium chloride and hydroxide [47] with solid to solution ration 1:20 w/w. After swelling the solid was centrifuged and washed with water 3 times by decantation, dispersion in water and centrifugation (5-10 min at 4000 rpm). Drying was carried out at 65 °C.

Surfactant extraction (deswelling) – 0.5-1 g of swollen solid was contacted without heating with 10 g of 20-25 % aqueous solution of ammonium nitrate in 15 ml of ethanol.

Pillaring: samples of the swollen material and TEOS, 1:100 w/w ratio, were stirred overnight. Reflux condenser was attached to the flask during the pillaring at elevated temperature. The solids were isolated by centrifugation or filtration through a frit. The isolated wet solid was kept in air until completely dry (1-3 days).

Calcinations were carried out for 4-8 hrs at 550 °C with ramp at 2 °C/min.

Characterization

X-ray powder diffraction (XRD) measurements were carried out using a Philips X'Pert diffractometer APD and a Bruker AXS D8 Advance diffractometer with CuKα radiation (λ = 0.154 nm) with steps of 0.02°.

Nitrogen adsorption/desorption isotherms were measured on a Micromeritics GEMINI II 2370 volumetric Surface Area Analyzer at liquid nitrogen temperature (-196 °C) to determine surface area,

View Article Online
DOI: 10.1039/C7DT03718J

pore volume and pore size distribution. Prior to the sorption measurements, all samples were degassed on a Micromeritics FlowPrep060 instrument under helium at 250 °C (heating rate 10 °C/min) for 6 h.

The surface area (S_{BET}) was calculated using adsorption data in the range of relative pressures p/p_0=0.05-0.2. The *t*-plot method was applied to determine the external surface area (S_{EXT}) and the volume of micropores (V_{MIC}). The adsorbed amount at relative pressure p/p_0=0.95 reflects the total adsorption capacity (V_{TOT}). Density Functional Theory (DFT) using standard Micromeritics software for cylindrical pores in an oxide surface for nitrogen at -196 °C was applied to calculate the pore size distribution.

Adsorption isotherms of argon at -186 °C were measured for selected samples on a Micromeritics ASAP 2020 volumetric instrument. In order to attain necessary accuracy in the accumulation of adsorption data, the instrument was equipped with three pressure transducers covering the 13.3 Pa, 1.33 kPa and 133 kPa ranges. Prior to the sorption measurements, all samples were degassed under the turbomolecular pump vacuum. Starting at an ambient temperature up to 110 °C (heating rate 1 °C/min) until the residual pressure of 1 Pa was achieved. After further heating at 110 °C for 1 h, the temperature was increased to 250 °C (1 °C/min) and maintained for 6 h. Non-Local Density Functional Theory (NLDFT) using standard Micromeritics software for cylindrical pores (Ar on oxides at -186 °C) was applied to estimate the micropore volume (V_{MIC}) and pore size distribution (D_{MIC}).

QE-TPDA measures the amount of sorbate desorbed or adsorbed by a sample as a function of temperature which is changing cyclically. QE-TPDA measurements of nonane (Sigma-Aldrich, >99 %, used without further purification) were performed with the use of the thermodesorption apparatus equipped with a thermal conductivity detector (Micro Volume TCD, Valco). Prior to the QE-TPDA experiment a sample (ca. 6-10 mg) was activated by heating in He flow (10 °C/min to 500 °C). The initial adsorption was carried out at room temperature by replacing pure helium used as the carrier gas with helium saturated with vapor of nonane (ca. 0.5 vol % at 25 °C). After adsorption was completed, the QE-TPDA experiment was performed by cyclic heating and cooling the sample (2 °C/min to 200 °C) in He/hydrocarbon flow (6.5 cm^3/min). The pore volume calculations were carried out by integration of the experimental desorption maxima and adjustment based on the calibration data. The density of nonane was assumed to be equal to that of the liquid (0.718 g/cm^3). Pore size distributions were calculated from the desorption parts of the QE-TPDA profiles according to the modified BJH scheme.[54]

C_s-corrected STEM – Prior to electron microscopy analysis the samples, in powder form, were deeply crushed using mortar and pestle. The fine divided material was dispersed in ethanol and few drops of the solution were placed onto carbon coated copper microgrids. The electron microscopy observations were performed using a spherical aberration corrected transmission electron microscopy XFEG FEI Titan operated at 300 kV. The column was fitted with a CEOS corrector for the electron probe allowing a nominal resolution of 0.8 Å. All data was acquired in STEM mode using a HAADF detector as previously reported.[56]

Solid state Magic-Angle-Spinning Nuclear Magnetic Resonance (MAS-NMR) spectra were acquired on the APOLLO console (Tecmag) at the magnetic field of 7.05 T (Magnex). For the ^{29}Si MAS NMR spectra a

View Article Online
DOI: 10.1039/C7DT03718J

3 μs rf pulse ($\pi/2$ flipping angle) was used, 4 kHz spinning speed, and 256 scans with the delay of 40 s were acquired.

Acknowledgements

M.K. and J.Č. thanks the Czech Science Foundation for the financial support 17-01440S. The financial support of the Narodowe Centrum Nauki Poland (2014/15/B/ST5/04498) is acknowledged. M.M. acknowledges OP VVV "Excellent Research Teams", project No. CZ.02.1.01/0.0/0.0/15_003/0000417 – CUCAM (Charles University Centre of Advanced Materials). A. M. acknowledges FEDER-Construyendo Europa desde Aragón for funding.

References

1. M. S. Whittingham and A. J. Jacobson, *Intercalation Chemistry*, Academic Press, New York, 1982.
2. D. O'Hare, in *Inorganic Materials*, eds. D. W. Bruce and D. O'Hare, Wiley, New York, 2nd edn., 1997, pp. 172-254.
3. A. Lerf, *Dalton Trans.*, 2014, 43, 10276-10291.
4. J. Rouquerol, F. Rouquerol, P. Llewellyn, G. Maurin and K. S. W. Sing, *Adsorption by Powders and Porous Solids: Principles, Methodology and Applications*, Elsevier Science, 2013.
5. R. T. Yang, *Gas Separation by Adsorption Processes*, Elsevier Science, 2013.
6. O. Deutschmann, H. Knözinger, K. Kochloefl and T. Turek, in *Ullmann's Encyclopedia of Industrial Chemistry*, Wiley, 2009, DOI: 10.1002/14356007.a05_313.pub2, pp. 1-110.
7. I. Fechete, Y. Wang and J. C. Védrine, *Catal. Today*, 2012, 189, 2-27.
8. M. Opanasenko, W. Roth and J. Cejka, *Catal. Sci. Technol.*, 2016, 6, 2742-2753.
9. G. Lagaly, M. Ogawa and I. Dékány, *Developments in Clay Science*, 2013, 5, 435-505.
10. W. Müller-Warmuth and R. Schöllhorn, *Progress in Intercalation Research*, Kluwer, Dordrecht, 1994.
11. J. Čejka, A. Corma and S. I. Zones, eds., *Zeolites and Catalysis: Synthesis, Reactions and Applications*, Wiley, 2010.
12. W. O. Haag, R. M. Lago and P. B. Weisz, *Nature*, 1984, 309, 589-591.
13. J. Weitkamp and L. Puppe, eds., *Catalysis and Zeolites: Fundamentals and Applications*, Springer, Berlin, 1999.
14. A. F. Masters and T. Maschmeyer, *Microporous Mesoporous Mater.*, 2011, 142, 423-438.
15. R. A. Schoonheydt, in *Stud. Surf. Sci. Catal.*, 1991, vol. 58, pp. 201-239.
16. M. E. Landis, B. A. Aufdembrink, P. Chu, I. D. Johnson, G. W. Kirker and M. K. Rubin, *J. Am. Chem. Soc.*, 1991, 113, 3189-3190.
17. M. K. Rubin and P. Chu, *Composition of Synthetic Porous Crystalline Material, Its Synthesis and Use*, *US Patent,* 4,954,325, 1990.
18. M. E. Leonowicz, J. A. Lawton, S. L. Lawton and M. K. Rubin, *Science*, 1994, 264, 1910-1913.
19. W. J. Roth, C. T. Kresge, J. C. Vartuli, M. E. Leonowicz, A. S. Fung and S. B. McCullen, *Stud. Surf. Sci. Catal.*, 1995, 94, 301-308.
20. L. Schreyeck, P. Caullet, J. C. Mougenel, J. L. Guth and B. Marler, *Microporous Materials*, 1996, 6, 259-271.
21. W. J. Roth and J. Čejka, *Catal. Sci. Technol.*, 2011, 1, 43-53.
22. W. J. Roth, P. Nachtigall, R. E. Morris and J. Čejka, *Chem. Rev.*, 2014, 114, 4807–4837.
23. W. J. Roth, B. Gil and B. Marszalek, *Catal. Today*, 2014, 227, 9-14.
24. B. Marler and H. Gies, *Eur. J. Mineral.*, 2012, 24, 405-428.

View Article Online
DOI: 10.1039/C7DT03718J

25. F. S. O. Ramos, M. K. de Pietre and H. O. Pastore, *RSC Adv.*, 2013, 3, 2084-2111.
26. W. J. Roth, *Stud. Surf. Sci. Catal.*, 2007, 168, 221-239.
27. W. J. Roth, B. Gil, W. Makowski, B. Marszalek and P. Eliasova, *Chem. Soc. Rev.*, 2016, 45, 3400-3438.
28. M. Choi, K. Na, J. Kim, Y. Sakamoto, O. Terasaki and R. Ryoo, *Nature*, 2009, 461, 246-249.
29. K. Na, W. Park, Y. Seo and R. Ryoo, *Chem. Mater.*, 2011, 23, 1273-1279.
30. W. J. Roth, P. Nachtigall, R. E. Morris, P. S. Wheatley, V. R. Seymour, S. E. Ashbrook, P. Chlubná, L. Grajciar, M. Položij, A. Zukal, O. Shvets and J. Čejka, *Nat. Chem.*, 2013, 5, 628-633.
31. P. Eliášová, M. Opanasenko, P. S. Wheatley, M. Shamzhy, M. Mazur, P. Nachtigall, W. J. Roth, R. E. Morris and J. Čejka, *Chem. Soc. Rev.*, 2015, 44, 7177-7206.
32. M. Mazur, P. S. Wheatley, M. Navarro, W. J. Roth, M. Položij, A. Mayoral, P. Eliášová, P. Nachtigall, J. Čejka and R. E. Morris, *Nat. Chem.*, 2016, 8, 58-62.
33. W. J. Roth, O. V. Shvets, M. Shamzhy, P. Chlubna, M. Kubu, P. Nachtigall and J. Čejka, *J. Am. Chem. Soc.*, 2011, 133, 6130-6133.
34. U. Díaz and A. Corma, *Dalton Trans.*, 2014, 43, 10292-10316.
35. K. Varoon, X. Y. Zhang, B. Elyassi, D. D. Brewer, M. Gettel, S. Kumar, J. A. Lee, S. Maheshwari, A. Mittal, C. Y. Sung, M. Cococcioni, L. F. Francis, A. V. McCormick, K. A. Mkhoyan and M. Tsapatsis, *Science*, 2011, 334, 72-75.
36. M. Osada and T. Sasaki, *Polym. J.*, 2015, 47, 89-98.
37. W. J. Roth and D. L. Dorset, *Structural Chemistry*, 2010, 21, 385-390.
38. P. Wu, J. F. Ruan, L. L. Wang, L. L. Wu, Y. Wang, Y. M. Liu, W. B. Fan, M. Y. He, O. Terasaki and T. Tatsumi, *J. Am. Chem. Soc.*, 2008, 130, 8178-8187.
39. W. B. Fan, P. Wu, S. Namba and T. Tatsumi, *Angew. Chem. Int. Ed.*, 2004, 43, 236-240.
40. T. Ikeda, Y. Akiyama, Y. Oumi, A. Kawai and F. Mizukami, *Angew. Chem. Int. Ed.*, 2004, 43, 4892-4896.
41. D. L. Dorset and G. J. Kennedy, *J. Phys. Chem. B*, 2004, 108, 15216-15222.
42. R. Millini, L. C. Carluccio, A. Carati, G. Bellussi, C. Perego, G. Cruciani and S. Zanardi, *Microporous Mesoporous Mater.*, 2004, 74, 59-71.
43. R. P. D. Graham, *Proceedings and transactions of the Royal Society of Canada, 3rd series*, 1918, 12, 185-190.
44. C. Marcilly, in *Encyclopedia of Supramolecular Chemistry*, eds. J. L. Atwood and J. W. Steed, CRD press, M. Dekker, 2004, pp. 1599-1609.
45. W. J. Roth and D. L. Dorset, *Microporous Mesoporous Mater.*, 2011, 142, 32-36.
46. B. Marler, Y. Wang, J. Song and H. Gies, *Dalton Trans.*, 2014, 43, 10396-10416.
47. W. J. Roth, B. Gil, W. Makowski, A. Sławek, J. Grzybek, M. Kubu and J. Čejka, *Chem. Mater.*, 2016, 28, 3616-3619.
48. W. J. Roth and C. T. Kresge, *Microporous Mesoporous Mater.*, 2011, 144, 158-161.
49. M. K. Rubin, *Crystalline borosilicate USA Patent,* 5,063,037, 1991.
50. Z. Zhao, W. Zhang, P. Ren, X. Han, U. Mueller, B. Yilmaz, M. Feyen, H. Gies, F.-S. Xiao, D. De Vos, T. Tatsumi and X. Bao, *Chem. Mater.*, 2013, 25, 840-847.
51. A. Burton, R. J. Accardi, R. F. Lobo, M. Falcioni and M. W. Deem, *Chem. Mater.*, 2000, 12, 2936-2942.
52. P. Chlubna, W. J. Roth, H. F. Greer, W. Z. Zhou, O. Shvets, A. Zukal, J. Cejka and R. E. Morris, *Chem. Mater.*, 2013, 25, 542-547.
53. W. Makowski, K. Mlekodaj, B. Gil, W. J. Roth, B. Marszałek, M. Kubu, P. Hudec, A. Smiešková and M. Horňáček, *Dalton Trans.*, 2014, 43, 10574-10583.
54. W. Makowski, L. Chmielarz and P. Kuśtrowski, *Microporous Mesoporous Mater.*, 2009, 120, 257-262.

View Article Online
DOI: 10.1039/C7DT03718J

55. W. Makowski and P. Kustrowski, *Microporous Mesoporous Mater.*, 2007, 102, 283-289.
56. A. Mayoral, J. Coronas, C. Casado, C. Tellez and I. Diaz, *Chemcatchem*, 2013, 5, 2595-2598.

View Article Online
DOI: 10.1039/C7DT03718J

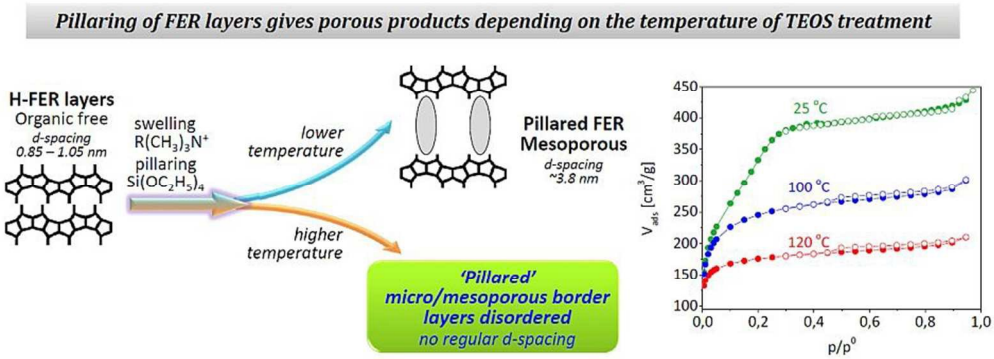

80x30mm (300 x 300 DPI)